Journal of Nanophotonics

Nanophotonics.SPIEDigitalLibrary.org

Optical modulators and beam steering based on electrically tunable plasmonic material

Kaifeng Shi
Zhaolin Lu

SPIE.

Optical modulators and beam steering based on electrically tunable plasmonic material

Kaifeng Shi* **and Zhaolin Lu**
Rochester Institute of Technology, Microsystems Engineering, Kate Gleason College of Engineering, Rochester, New York 14623, United States

Abstract. Surface plasmon based photonic (or plasmonic) circuits merge electronics and photonics at the nanoscale, creating the ability to combine the superior technical advantages of photonics and electronics on the same chip. Recent work has demonstrated their remarkable applications in subwavelength optics, data storage and transmission, light harvesting and generation, and microscopy, as well as bioapplications. Plasmonics has become one of the most intensive research subjects in recent years, and much effort has been made to develop novel and efficient waveguiding structures and plasmonic materials. We will first review some major progress in subwavelength plasmonic waveguides and plasmonic materials. Then, focusing on the applications of a class of promising alternative plasmonic materials, transparent conducting oxides, we will introduce some of our up-to-date study, especially on electro-absorption modulators and beam steering. [DOI: 10.1117/1.JNP.9.093793]

Keywords: nanoplasmonics; plasmonic materials; transparent conducting oxides; electro-absorption modulators.

Paper 14111SS received Oct. 7, 2014; accepted for publication Dec. 17, 2014; published online Jan. 20, 2015.

1 Introduction

Surface plasmons (SPs) are electromagnetic waves propagating along metal-dielectric interfaces. These light waves are trapped at the interfaces because of their resonant interaction with the mobile electrons of the conductor. As a result, SPs have the extraordinary ability to confine light in the nanometer scale. On the other hand, traditional photonic devices, such as dielectric waveguides, have suffered from the diffraction limit, which hinders some applications of photonics in communications, sensing, imaging, etc. Inevitably, a marriage between SPs and photonics leads to an exciting branch: plasmonics, named by a research group in Caltech in 2000.[1] Although plasmonics has not been a widely investigated topic for more than two decades, the recognition of SPs can be traced back to Riechie's work in the 1950s.[2] He further illustrated light scattering from nanoscale metallic particles in the 1970s.[3] The development of nanofabrication techniques has given researchers the ability to realize complicated structures with a variety of property-controllable materials. Besides, high-performance computational tools have greatly facilitated the prediction and approximation of newly designed structures and devices. People have been equipped to explore the in-depth behaviors of nanoplasmonic devices and systems in optical communications and information exchange, and have made plasmonics a highly developed and advanced science.[4] In this article, we will first review the development of plasmonic waveguides and the current progress of novel plasmonic materials, and then will focus on electro-optic (EO) modulators based on plasmonic materials, especially our up-to-date work utilizing transparent conducting oxides.

*Address all correspondence to: Kaifeng Shi, E-mail: kxs9364@rit.edu

2 Plasmonic Waveguides

Aiming at guiding light in the subwavelength or even deep subwavelength scale, many different kinds of plasmonic waveguiding structures have been proposed and studied since the 1990s.[5] Typical configurations include metallic nanowires[6,7] and metallic nanoparticle arrays.[8,9] Such configurations support a highly confined mode and might be ideal systems for two-dimensional (2-D) confinement,[10] but they suffer from high loss and most of them work only near the SP frequency. Another conventional plasmonic waveguide is thin metallic slabs embedded in a homogeneous dielectric medium, or an insulator/metal/insulator (IMI) waveguide, which could allow SPs to propagate tens of centimeters at infrared frequencies. However, the associated fields cannot be strongly confined in the transverse direction.[11,12] The inverse structure to IMI, or the MIM waveguide, might be a satisfactory compromise: it provides both good confinement and acceptable propagation length, and it has also been shown to support a nanoscale modal size at frequencies ranging from dc to visible.[13,14] Even more waveguide structures have been investigated to deal with the trade-off between the confined modal size and propagation losses: metal wedge,[15] dielectric loaded metal,[16] channel,[17] and hybrid plasmonic waveguide.[18] Besides the effort made in designing more reasonable waveguiding structures, people have also been eagerly exploring novel plasmonic materials that can help device performance in all aspects. The next section is a brief review of typical materials for plasmonic applications.

3 Plasmonic Materials

Microelectronics could not develop without silicon, nor does plasmonics without proper materials. Metals are commonly used plasmonic materials with advantages of high conductivity and small ohmic losses.[19] However, popular metals, such as gold and silver, have high optical losses due to both intraband and interband transitions, which has been the major obstacle in the design of efficient devices.[20,21] Besides, metals suffer from other shortcomings. For instance, (1) the fabrication process of thin metal films is challenging;[22,23] (2) metals, e.g., copper and silver, face degradation problems when exposed to air or humidity;[24,25] (3) the dielectric permittivity of metals is almost unadjustable because of their ultrahigh carrier concentrations. The utilization of novel plasmonic materials could not only overcome the bottleneck of high losses, but also provide other advantages, such as design flexibility, easy fabrication and integration as well as tunability. The choice of a specific material depends on the desired working frequency and application. Typical alternative plasmonic materials include conventional semiconductors, metal compounds, and 2-D materials, such as graphene.

3.1 *Conventional Semiconductors*

Conventional semiconductors, such as silicon, germanium, and III-V semiconductors, have been thoroughly studied and widely applied in the microelectronic and optoelectronic industries. Since integrating plasmonic devices on the mature and developed platforms provided by conventional semiconductors is an inevitable trend, it is of great importance to explore and realize the potential for plasmonic properties from conventional semiconductors. The solution is a widely known technique: doping. The free carrier concentration in doped semiconductors in industry is usually smaller than 10^{17} cm^{-3}, far less than that in metals, which is in the order of 10^{22} cm^{-3} (Ref. 5). In order to achieve semiconductor plasmonics, a much higher doping level is a necessity. Some research on highly doped semiconductors exhibiting metallic behavior has already been reported.[26–30] However, the solid solubility in conventional semiconductors sets an upper limit for the doping level. For example, it is almost impossible to achieve a carrier concentration of 10^{21} cm^{-3} in silicon.[19] As a result, plasmonics based on conventional semiconductors could work only at mid-infrared (MIR) or even a lower frequency regime. It is still challenging to use conventional semiconductors for near-infrared (NIR) applications.

3.2 *Metal Compounds*

As it needs abundant free carriers to support SPs, most of the alternative plasmonic materials contain a metal component. On the other hand, compared with metals, the carrier concentration in these materials has been reduced due to nonmetallic elements, which would result in lower optical losses. Silicides, germanides, and metal nitrides are typical metal compounds used as plasmonic materials. These materials are important and are also advantageous from the perspective of standard fabrication methods and integration with existing CMOS platforms.[19] Besides, they offer the possibility to be optically tuned by varying their composition. According to previous studies,[31–35] they do not perform better than noble metals as plasmonic materials. However, they have a great potential to be optimized by exploring more complicated compounds or better compositions.

Transparent conducting oxides (TCOs) are doped metal oxides that receive much research focus. They have a large bandgap, which make them visibly transparent. They can be heavily doped to exhibit high electrical conductivity, and more importantly, their plasma frequencies lie in the NIR regime. The exploration of TCOs as the plasmonic metamaterial for NIR applications can be traced back to decades ago.[36–38] Some comparative studies have been reported.[19,32,39,40] Indium tin oxide (ITO), a well-known representative of TCOs, has been widely used as transparent electrodes in solar cells and for displays.[41–44] The carrier concentration in TCOs can be controlled by manipulating the concentration of oxygen vacancies and interstitial metal dopants, which result a change in optical properties. TCOs can be fabricated with a standard physical vapor or chemical vapor deposition process and integrated with other standard technologies. ITO is expensive due to the limited source of indium. Other widely investigated TCOs include aluminum zinc oxide (AZO), gallium zinc oxide, and so forth.[39,45] TCOs have been shown as a promising candidate for tunable plasmonic devices. Some applications of TCOs as tunable plasmonic materials, especially in EO modulators, will be further addressed in this article.

3.3 *2-D Materials*

In recent years, great effort has been made on the investigation of 2-D plasmonic materials, especially graphene.[46–50] Their unique properties have made them attractive in many applications.[51–56] Graphene-based plasmonics for surface-enhanced Raman spectroscopy, photodetection, modulation, and sensing has been predicted,[57–60] mainly relying on the tunability of its optical conductivity. Other 2-D atomic crystals under investigation for plasmonic applications include MoS_2, BN, TaS_2, $NbSe_2$, and WS_2.[53,61,62] The major problem for 2-D materials is the difficulty in mass production. Besides, their application in NIR or visible range still remains a challenge.

4 EO Modulators Based on Plasmonic Materials

4.1 *Introduction*

As one of the most critical devices in optoelectronic integrated circuits, EO modulators have long been suffering from the poor EO properties of conventional materials, even for some well-known EO materials, such as lithium niobate,[63,64] which inhibit significant modulation within a compact modulator. Some phase modulators are on the order of millimeters.[65,66] In recent years, many EO modulators have been proposed for the purpose of a small footprint and better performance. For instance, silicon resonator modulators enhance the EO effect due to the large quality factor of the resonant cavity and, thus, can shrink their dimensions to tens of micrometers.[67–69] However, resonator modulators usually suffer from bandwidth limitation and temperature fluctuation as well as fabrication tolerance. On the other hand, nonresonant modulators exhibit broadband performance, but they lose compactness.[70]

Development in plasmonics also opens a new vista for EO modulators.[71–75] Some EO modulators utilize a metal-oxide-semiconductor (MOS) structure and show a hybrid plasmonic mode,[75,76] thus having the advantages of lower losses and easy integration with CMOS platforms. A recent reported plasmonic phase modulator has a very small length (29 μm) and

high speed (40 Gbit/s), which realizes EO modulation by exploiting the Pockel effect in nonlinear polymer.[70] The choice of an active EO material is another important concern that affects device performance. In addition to lithium niobate, silicon, and polymers, graphene has also been reported as an active material for a nanoscale EO modulator working around telecommunication wavelengths.[77] As previously mentioned, the family of TCOs plays an important role in novel EO modulators.

The optical dielectric constant of TCOs can be approximated by the Drude model:

$$\varepsilon = \varepsilon' + j\varepsilon'' = \varepsilon_\infty \left[1 - \frac{\omega_p^2}{\omega(\omega + j\gamma)}\right], \tag{1}$$

where ε_∞ is the high-frequency dielectric constant, ω is the angular frequency of the light wave, and γ is the damping coefficient of free carriers related to optical losses. The plasma frequency is defined by

$$\omega_p = \sqrt{\frac{Ne^2}{\varepsilon_\infty \varepsilon_0 m^*}}, \tag{2}$$

which depends on carrier concentration N and the electron effective mass m^*. According to the above equations, the optical material's dielectric constant shifts with different carrier concentrations. In Ref. 78, the unity-order index change of ITO film in an MOS structure is reported by voltage-induced accumulation carriers at the ITO-insulator interface. Therefore, by engineering the carrier concentrations in TCOs, the absorption of active material, which is directly related to its index, or dielectric constant, could be tuned. TCOs are widely used in electro-absorption (EA) modulators.[79–81]

The absorption coefficient of some specific materials can also tuned by optical signals, which leads to another kind of plasmonic modulator, namely all-optic modulators.[82–84]

4.2 *EA Modulators Based on ITO MOS-Like Structure*

4.2.1 *ITO/Electrolyte Gel modulator*

In our recent study,[85] we employed a similar structure as MOS but replaced the sandwiched oxide material with electrolyte gel to form simple multilayer modulators based on ITO. The interface between a metal (or heavily doped semiconductor) and electrolyte is of interest in most electrolyte applications, where two parallel layers of positive and negative charges called an electric double layer (EDL) are formed. To some degree, an electrolyte can be treated as a medium with a huge dielectric constant. Another advantage of using an electrolyte as the gating material is that the device behavior can be conveniently controlled by varying the concentration of chemical compounds in the electrolyte.[86,87]

We fabricated an ITO film on transparent glass by physical vapor deposition. After applying a thin layer of electrolyte gel on the surface of the ITO, a heavily doped silicon chip or another identical ITO sample with the ITO side facing the electrolyte gel is tightly pushed toward the substrate ITO to form the multilayer modulator, as shown in the inset of Figs. 1(a) and 1(b), respectively.

We built an experimental setup[56] to measure the light reflectance of the modulators by sweeping the incident angle. The reflectance was measured in a sequence of (1) without an externally applied voltage, (2) with an externally applied voltage V_P, and (3) with an externally applied voltage that has a reversed polarity but the same magnitude. The modulation depth, $M(\theta_1)$, is defined as: $M(\theta_1) = |R_{+Vp} - R_{-Vp}|/R_0$, where R_0 is the measured reflectance without an applied voltage, and $|R_{V_P} - R_{-V_P}|$ is the magnitude of the difference of the two reflectances with applied voltages. For $\lambda = 1520$ nm TM-polarized light, the modulation depth at a specific angle of $\theta_1 = 70$ deg can be calculated as $M(70\ \text{deg}) = 20.7\%$, as shown in Fig. 1(a). The double EDLs shown in Fig. 1(b) result in an even higher modulation depth, $M(70\ \text{deg}) = 38.8\%$, with TE-polarized light at $\lambda = 1520$ nm. We attribute the modulation to the change of the free carrier concentration in either the 5-nm-thick depletion layer or accumulation

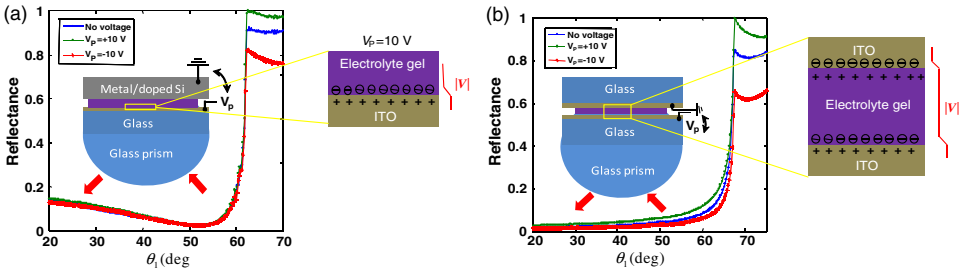

Fig. 1 Reflectance as a function of incident angle for (a) the heavily doped Si/electrolyte gel/indium tin oxide (ITO) and (b) the ITO/electrolyte gel/ITO modulators with different applied voltages. Inset: illustration of the modulators.

layer in the ITO at the interface, which is assisted by the redistribution of the ions in electrolyte gel induced by the applied voltage. The results also show that the ITO-based multilayer modulator is not sensitive to the polarization of the incident light beam.

The measured reflectance of the ITO modulator was numerically fitted by calculating the reflectance through the multilayer structure based on the transfer matrix method.[88] Table 1 summarizes the carrier concentration and corresponding dielectric constant of the active ITO layer (5 nm) induced by an externally applied voltage at $\lambda = 1520$ nm.

The switching speed of the modulator is directly influenced by the relaxation of the ions in the electrolyte gel. For the modulator structure shown in Fig. 1(a), another experiment was carried out to test this relaxation effect.

As shown in Fig. 2, we applied a 30 s positive pulse at time t_1 and a 30 s negative pulse at t_2. We can observe relatively fast modulation when the pulses are excited; however, a very long time is needed for the ITO-gel modulator to recover to the baseline level. The phenomenon could be caused by the different mobilities of the major carriers in the 5-nm region in the ITO at the interface. Both the ions in the electrolyte gel and the free carriers in the ITO needed to form the EDL will probably limit its applications at high frequencies. This experiment was conducted with $\lambda = 1310$ nm TM-polarized light, where the modulation depth $M(65\ \text{deg}) = 12.4\%$, so the ITO/electrolyte gel modulator is a potential broadband device. The problem is the modulator has a short lifetime and a very slow switching speed.

4.2.2 *ITO/HfO$_2$/Al modulator*

In order to make more efficient modulators, we apply high-k dielectric material in our designed EO modulator structure,[85,89] as illustrated in Fig. 3(a). High-k material HfO_2 is utilized as the gate oxide for its ultrahigh permittivity as well as process stability.[90] Aluminum is chosen here for its excellent conductivity, low absorption in the NIR regime, as well as low cost. Another advantage of using an aluminum layer is that light absorption can be directly measured by $1 - R$ (R is the power reflectance).

The modulator was measured the same way as the ITO/electrolyte gel modulator. The measured reflectance as a function of the incident angle at different wavelengths is shown in Figs. 3(c)–3(f). The results were also numerically fitted to find the change of the optical constant of the active ITO layer. The fitting parameters of the active ITO layer (5 nm), together with further Drude model fitting curves, are shown in Fig. 3(b). From Fig. 3, broadband EO modulation has

Table 1 Carrier concentration and dielectric constant of active Indium tin oxide (ITO) layer.

Voltage (V)	Carrier concentration (cm^{-3})	Dielectric constant
0	$N_0 = 9.82 \times 10^{20}$	$\varepsilon_{\text{untuned}} = 3.7 + j1.0$
10	$N_{\text{dep}} = 5.34 \times 10^{20}$	$\varepsilon_{\text{dep}} = 4.23 + j0.5$
−10	$N_{\text{acc}} = 4.75 \times 10^{21}$	$\varepsilon_{\text{acc}} = -0.47 + j4.9$

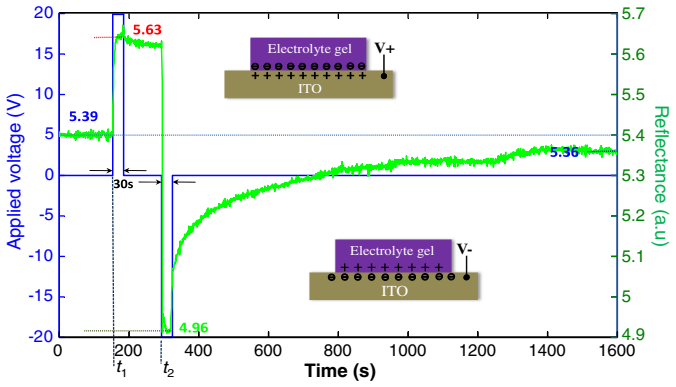

Fig. 2 Ionic relaxation effect of the electrolyte gel, at an angle of $\theta_1 = 65$ deg.

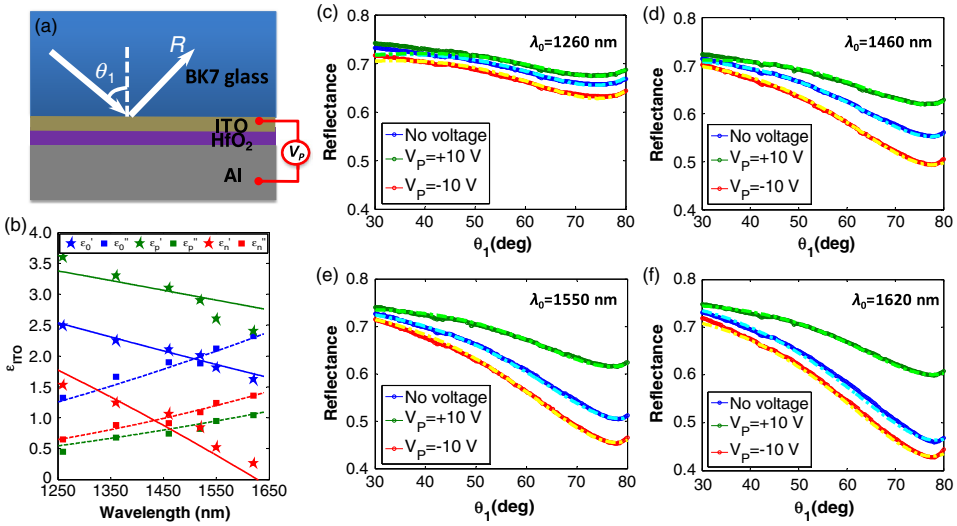

Fig. 3 (a) Schematic for ITO/HfO_2/Al modulator. (b) Fitting dielectric constant (real and imaginary part) of active ITO layer (the rest ITO layer keeps untuned with the value of the blue markers): blue, green, and red markers correspond to parameters with zero bias, positive bias, and negative bias, respectively; solid and dashed lines are from further fitting by the Drude model. (c) to (f) Reflectance as a function of incident angle for the modulator under different applied voltages for different wavelengths (solid lines) and the fitting curves (dashed lines).

been achieved and the largest modulation depth obtained at a specific angle, $\theta_1 = 78$ deg, is $M_{\max}(78 \text{ deg}) = 37.42\%$ for $\lambda_0 = 1620$ nm. We call the angle where the maximum modulation depth is achieved the modulation angle.

We attribute the modulation mainly to the change of the free carrier concentration in the 5-nm-thick voltage-induced active layer in ITO. For instance, when a negative bias is applied, excess electrons will be induced at the ITO–HfO_2 interface, which results in carrier accumulation in the active ITO layer; on the contrary, the active layer will be depleted under a positive bias.

Besides, we examined the variation of modulation depth with regard to applied voltages of different magnitudes. Starting from 0 V, we measured the power reflectance at the modulation angle at a ± 2 V step. The measured results for $\lambda_0 = 1550$ nm are shown in Fig. 4(a). According to our observation, there may exist a threshold voltage around 2 V for the modulator to start working. After that, the modulation depth and applied voltage follow almost a linear relation.

Furthermore, we have investigated the modulation speed of the ITO/HfO_2/Al modulator. We observed two stages of modulation, namely, fast modulation and slow modulation, as shown in Figs. 4(b) and 4(c). In fast modulation, the reflectance almost instantly shifts up or down with the applied voltages and quickly recovers to the baseline level when turned to zero bias. However, the fast modulation contributes to a small magnitude of modulation depth. After

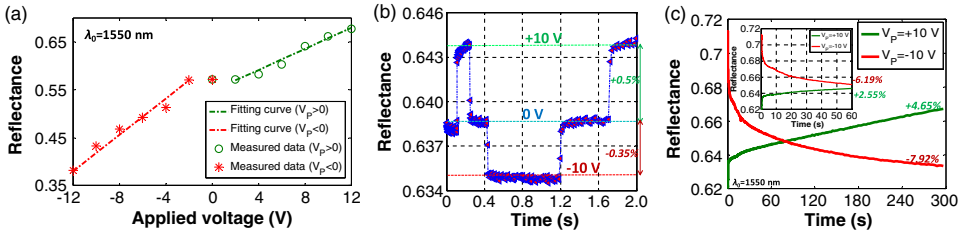

Fig. 4 (a) Power reflectance as a function of applied voltage at the modulation angle for $\lambda_0 = 1550$ nm. (b) and (c) Power reflectance as a function of time at the modulation angle for $\lambda_0 = 1550$ nm. (b) Fast modulation and (c) slow modulation. Inset: reflectance change within 60 s.

the first stage, the reflectance keeps increasing or decreasing under the applied voltage. We can see that the slope gets smaller and smaller as time elapses, which indicates a slower and slower absorption change. The imperfection in fabrication, the device resistance-capacitance (RC) delay, and the role of the ITO–HfO_2 surface states may be the factors that limit the performance of the modulator.

The ITO-based modulators could be very compact and work over a large wavelength spectrum. The switching speed still needs further optimization. In our study, another key point we are focusing on is tuning the active ITO into the dielectric constant epsilon-near-zero (ENZ) state, where the potentially largest modulation depth would be observed. In the next section, we will review some of our theoretical study on TCOs working as ENZ materials.

5 ENZ-Slot Waveguides Based on Transparent Conducting Oxides

5.1 *ENZ Material and Slot Waveguide*

The development of metamaterials enables material permittivity to be engineered to almost any arbitrary value.[91] Particularly, some recent research has been focused on ENZ, or index-near-zero material, which has a dielectric constant (or refractive index) with a small magnitude in a frequency range of interest. Novel applications of ENZ materials have been investigated, such as tunneling and squeezing electromagnetic energy through subwavelength narrow channels,[92,93] design of matched zero-index materials,[94,95] and shaping the radiation pattern of a source.[96,97]

According to the Drude model [Eqs. (1) and (2)], the ENZ effect of a material shows up when $\omega \approx \omega_p$. Metals have such a high plasma frequency that they exhibit a large real dielectric constant in NIR range. Most semiconductors have doping limitations that result in their plasma frequencies located beyond MIR. The appropriate carrier concentrations in TCOs (10^{19} to 10^{21} cm^{-3}), together with advantages of low intrinsic loss and tunable optical properties, as well as easy fabrication and integration, have made them excellent plasmonic materials in NIR.[19] Several other ENZ metamaterials have also been reported.[98–100]

In our recent work, we studied a structure combining ENZ material with a slot waveguide, namely ENZ-slot waveguide, and found some unprecedented properties. A slot waveguide[101,102] consists of a narrow low refractive index slot sandwiched at the center of a single-mode high-index waveguide, which can greatly confine light and enhance optical fields in the slot region. The slot waveguide works well only for the TM mode where the magnetic field is parallel to the slabs. When the free carrier effect is considered in complex dielectric constants, the continuity of electric flux density between two media holds, i.e., $\varepsilon_1 E_{1n} = \varepsilon_2 E_{2n}$ or $E_{1n} = (\varepsilon_2/\varepsilon_1)E_{2n}$. If ENZ materials were applied as the slot, enormous enhancement of the E-field would take place and more power could be confined in the ENZ-slot.

As a simple example showing field enhancement and power confinement of the ENZ-slot waveguide, the structure shown in Fig. 5(a) is analytically examined. Figure 5(b) plots the electromagnetic field intensity, power percentage in the slot, and effective index of the structure as a function of slot dielectric constant ε_{slot}. We can see the dramatic change of these terms when ε_{slot} is approaching zero. In particular, the effective index sharply decreases from 1.6 to ~1 when ε_{slot} decreases from 0.1 to nearly zero due to the larger power confinement within the low index slot.

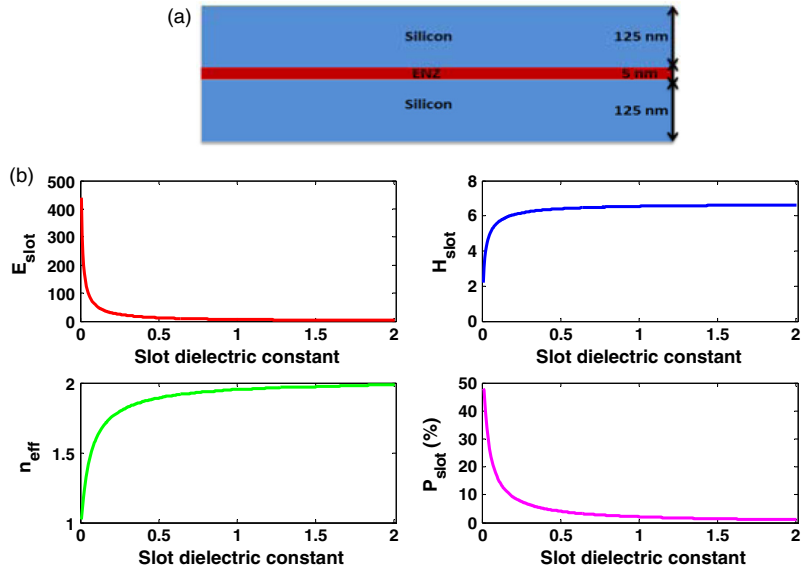

Fig. 5 (a) Structure of a simple three-layer waveguide (value of n_{silicon} used for $\lambda_0 = 1550$ nm is 3.47). (b) Plots of electric field, magnetic field, power percentage in the slot, and effective index of the structure versus slot dielectric constant.

5.2 *EA Modulators Based on TCO-Slot Waveguide*

According to the experimental data in Ref. 78, ITOs with different carrier concentrations could work as ENZ materials at specific wavelengths.[103] As shown in Fig. 6(a), the ENZ effect of ITO is achieved at $\lambda_0 = 1136$ nm and $\lambda_0 = 843$ nm under carrier concentrations $N_1 = 1.65 \times 10^{22}$ cm^{-3} and $N_2 = 2.77 \times 10^{22}$ cm^{-3}, respectively. As suggested, the accumulation of carriers could be realized by electric signal in an MOS-like structure [Fig. 6(b)], which indicates the optical tunability of ITO.

The dielectric constant of ITO at epsilon-far-from-zero (untuned) state and ENZ state is shown in Table 2, where we can see the magnitude has changed tens or even hundreds of times due to the externally applied voltage. The huge change in the magnitude of the dielectric constant may find applications in EA modulators. In dielectric heating theory, the power dissipation density can be written as

$$p_d = \frac{1}{2}\sigma E^2 \propto \frac{1}{2}\varepsilon'' E^2 \propto \frac{1}{2}\varepsilon''/|\varepsilon|^2, \tag{3}$$

which can be greatly enhanced when $|\varepsilon| \to 0$. Figure 6(b) depicts typical EA modulator configurations based on a TCO-slot waveguide. The modulator would be off with low absorption at

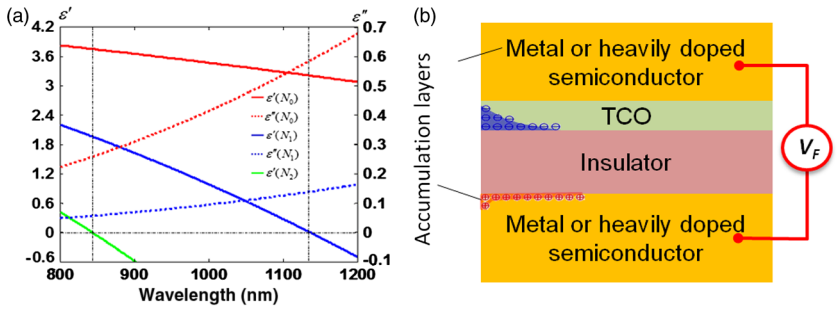

Fig. 6 (a) Real part of the dielectric constant of ITO as a function of wavelength at three different carrier concentrations based on the Drude model.[87] (b) Illustration of the epsilon-near-zero (ENZ)-slot waveguide.[80]

Table 2 Dielectric constant of ITO at untuned and epsilon-near-zero (ENZ) state.

Wavelength (nm)	ε_0	ε_{ENZ}
1136	$3.0274 + j0.586$	$-0.0014 + j0.1395$
843	$3.7541 + j0.2579$	0.0045

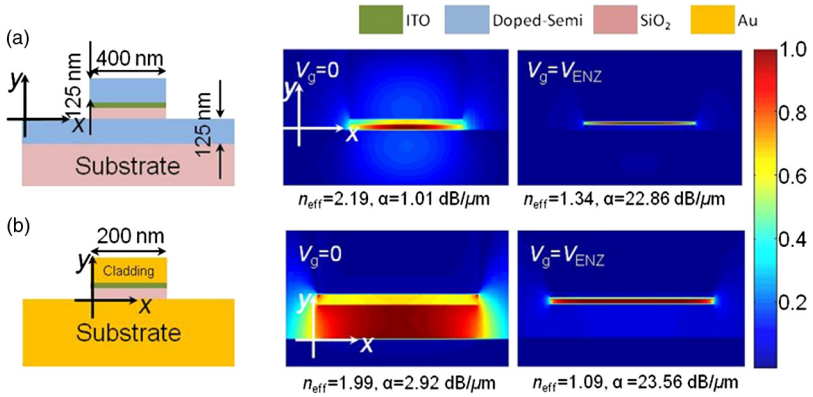

Fig. 7 The electric field profiles, effective indices, and propagation loss for different ITO-slot waveguide at untuned state and ENZ state, respectively: (a) in a dielectric rib waveguide and (b) in a plasmonic waveguide.

the untuned state and on with high absorption at the ENZ state, due to the change of the dielectric constant. Note that the working wavelength chosen for the EA modulators is $\lambda_0 = 1136$ nm.

ITO EA modulators based on a dielectric waveguide [Fig. 7(a)] and a plasmonic waveguide [Fig. 7(b)] were proposed and simulated. Their modes were solved by the finite-difference time-domain (FDTD) method. Note that we applied a 10-nm-thick ITO in the waveguides, of which 5 nm at the ITO–SiO_2 interface were assumed to be tuned. From the results, we can see significant field enhancement and confinement within the ENZ-slot and a considerable shift in the effective index. More importantly, a huge change in waveguide attenuation (21.85 dB/μm for dielectric waveguide and 20.64 dB/μm for plasmonic waveguide) is achieved.

The insertion loss of the EA modulators was evaluated by three-dimensional (3-D) FDTD simulation. For a 150-nm-long modulator embedded in a plasmonic rib waveguide, the insertion loss is 0.48 dB and the modulation depth is 3.42 dB, which is very close to the one predicted by the 3-D mode solver. A 200-nm-long modulator embedded in a dielectric rib waveguide shows an insertion loss of 0.56 dB and a modulation depth of 3.53 dB.

In Ref. 81, we utilized a similar theory and demonstrated EA modulation based on an ENZ-slot waveguide, where another TCO material, AZO, is serving as the tunable slot. We also showed that the optical bandwidth of these modulators can be over several terahertz due to slow Drude dispersion. These TCO-slot waveguide-based EA modulators are compact and could potentially work at ultrahigh speed, being mainly limited by the RC delay introduced by electric circuits.

Actually, the EA modulators we proposed in Sec. 4 are mainly based on this theoretical study, and we intend to search for the ENZ effect in an active ITO layer, which was supposed to produce the maximum modulation depth. According to the parameters in Table 1 and Fig. 3(b), more effort is still needed in optimizing the design and the fabrication process.

5.3 *Laser Beam Steering by TCO-Slot Waveguide*

In both the analytical calculation of a simple ENZ-slot waveguide in Sec. 5.1 and the numerical simulation of the EA modulators, we see that the effective indices of the waveguides undergo the considerable change. Thus, we can engineer the effective index of the ENZ-slot waveguide by

tuning the refractive index of ITO film. This phenomenon may find applications in laser beam steering.[91] Laser beam steering techniques are being widely investigated because of their applications in laser-based sensing, communication and power projection, and other fields. Mechanical and nonmechanical methods, such as beam steering with a rotating (Risley) prism, macro-optical mirrors, microlens arrays, and liquid crystal polarization gratings, have been proposed,[104–106] heading to the purposes of compactness, low power, high speed, lightweight, and a large field of regard. To advance this technique, we proposed a novel beam steering structure based on the tunable ENZ-slot waveguide.

In order to realize beam steering, we added periodic gratings on top of the ITO-slot waveguide [Fig. 8(a)] and made use of the tunable effective index of the structure to steer the incident laser beam. According to the grating equation,

$$k_0 \sin\theta + \frac{2\pi l}{\Lambda} = k_0 n_{\text{eff}} \Leftrightarrow \sin\theta + l\lambda_0/\Lambda = n_{\text{eff}}, \tag{4}$$

where λ_0 is the wavelength of the incident beam, $k_0 = 2\pi/\lambda_0$ is the wave number, Λ is the period of the gratings, $l = \{\pm 1, \pm 2 \ldots\}$ is an integer representing the propagating mode of interest, n_{eff} is the effective index of the waveguide, and θ is the steering angle. Given a fixed grating period and wavelength, the incident beam can be steered by tuning the effective index, which, as discussed above, is able to be fulfilled by electrically tuning the optical property of ITO.

For an incident beam of $\lambda_0 = 1136$ nm, the attenuation would be too large for the waveguide when ITO is at the ENZ state. Since long-distance propagation is a major concern here, in order to achieve easy detection we chose the working wavelength to be 843 nm, which is the cross-wavelength for ITO under N_2. Here the damping factor $\gamma \approx 0$,[78] so the attenuation of the ENZ-slot waveguide decreases quite a bit: $\alpha_0 = 0.328$ dB/μm when untuned and $\alpha_2 = 0.107$ dB/μm under N_2. Besides, the effective index is also significantly shifted from 2.29 to 1.65, which promises a wide steering angle.

For convenience, in Eq. (4), we assume $\Lambda = 653$ nm, $\lambda_0 = 843$ nm, and $l = 1$, which make $l\lambda_0/\Lambda = 1.29$. Figure 8(b) plots the complex effective index of the waveguide in terms of the carrier concentration. The effective index that can be obtained ranges from 1.53 to 3.22 (values >2.29 may correspond to a higher harmonic mode). Therefore, the value range for $\sin\theta$ that can be achieved is from 0.24 to 1, which also results in a steering angle θ from 14 to 90 deg. Note that

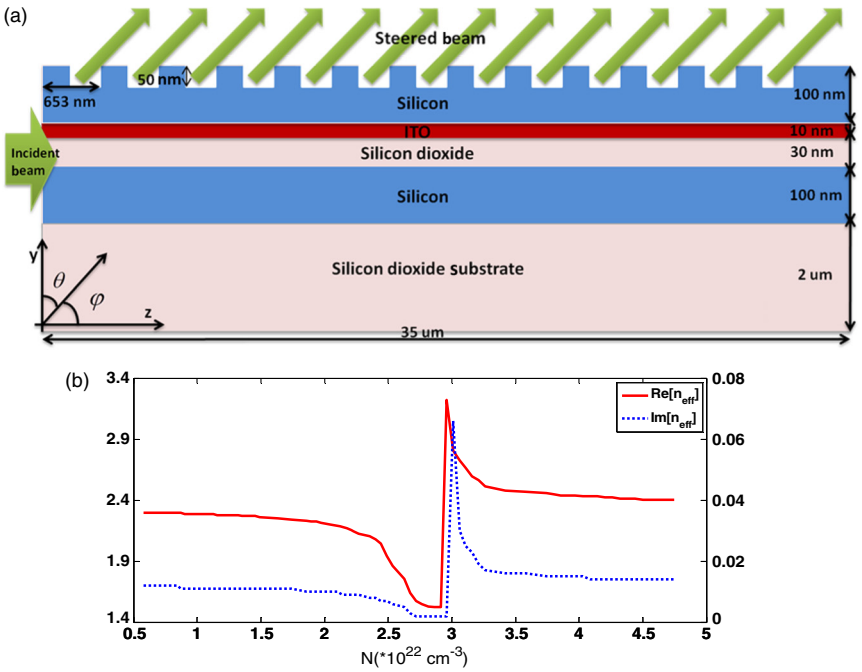

Fig. 8 (a) Illustration of beam steering based on ENZ-slot waveguide with periodic gratings. (b) Complex effective index in terms of carrier concentration.

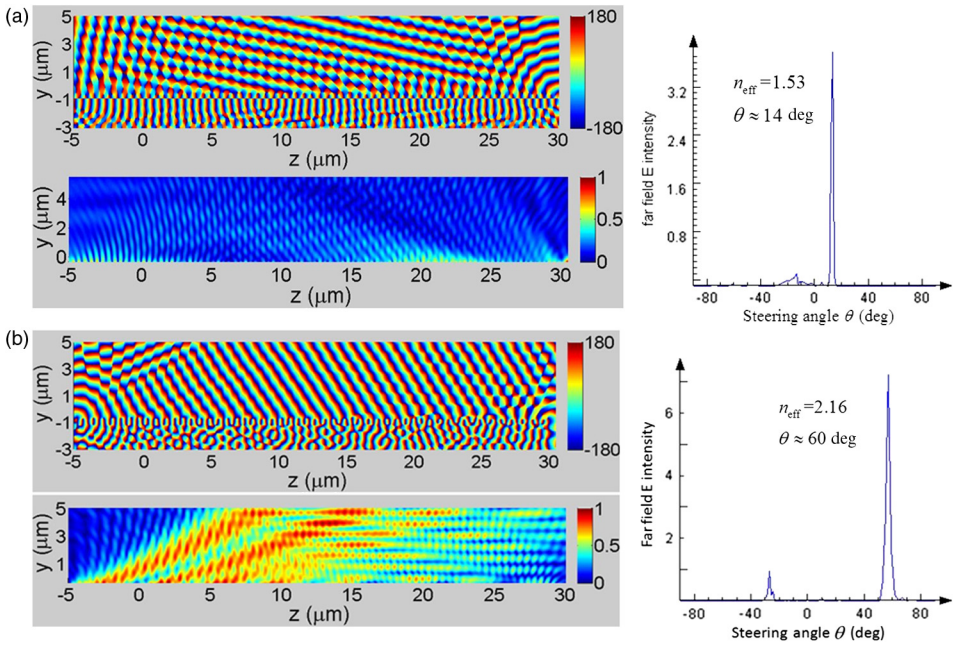

Fig. 9 Phase, normalized magnitude, and far-field intensity of E_y for steering angles of (a) 14 deg and (b) 60 deg.

the minimum effective index is achieved when the active ITO layer (5 nm) at the ITO–SiO_2 interface is at the ENZ state.

FDTD simulations were performed to verify the predictions. The phase plot, normalized intensity magnitude plot, and far-field intensity plot of the dominate electric field E_y for the steering angles of 14 and 60 deg are shown in Fig. 9.

The phase and magnitude plots illustrate the propagation direction of the steered beam in the near-field, which is normal to the phase line, or along the magnitude trend. Note that the magnitude plots show only the electric field above the ENZ-slot due to a much higher electric field in the slot. Far-field intensity plots can clearly identify the steering angle. According to the figures, laser beam steering is achieved by the effective index change of the ENZ-slot waveguide. The maximum steering angle we got from simulations is $\theta \approx 75$ deg.

As one example, we showed some theoretical studies of TCOs behaving as the ENZ material in ENZ-slot waveguides and their applications in EA modulation and laser beam steering. ENZ-slot waveguides highly confine electromagnetic fields in the slot region, so the behaviors of the waveguides can be greatly changed by tuning the slot material. Besides, they can be easily fabricated layer by layer. With the advantages of TCOs in low intrinsic loss, excellent tunability as well as ease of fabrication and integration, the combination, TCO-slot waveguides, is of great promise in building novel optoelectronic devices for NIR applications.

6 Conclusion

Assisted by modern fabrication techniques and computational tools, plasmonics has opened up new horizons for conventional electronics and photonics in almost every aspect. In this article, we briefly reviewed the current progress in plasmonic waveguide platforms and plasmonic materials, which serves as the key factor to allow science to be transformed into usable technologies. Then, based on TCOs, which nearly have all the properties that a novel plasmonic material requires, especially for NIR applications, we introduced some waveguiding structures and revealed their potentials to be EA modulators with compactness, ultrahigh speed, and easy fabrication. Another application of TCOs in laser beam steering was also presented. Although only preliminary results are provided here, we look forward to the successful development of such techniques, which may lead to a significant breakthrough in on-chip optical interconnects.

Acknowledgments

The publication was made possible by Grant Number W911NF-12-1-0451 from the United States Army. This material is based upon work partially supported by the National Science Foundation under Award No. ECCS-1308197.

References

1. H. A. Atwater, "The promise of plasmonics," *Sci. Am.* **296**, 56–63 (2007).
2. R. H. Ritchie, "Plasma losses by fast electrons in thin films," *Phys. Rev.* **106**, 874–881 (1957).
3. R. H. Ritchie, "Surface plasmons in solids," *Surf. Sci.* **34**, 1–19 (1973).
4. M. I. Stockman, "Nanoplasmonics: past, present, and glimpse into future," *Opt. Express* **19**, 22029–22106 (2011).
5. R. Yang and Z. Lu, "Subwavelength plasmonic waveguides and plasmonic materials," *Int. J. Opt.* **2012**, 258013 (2012).
6. J. C. Weeber et al., "Plasmon polaritons of metallic nanowires for controlling submicron propagation of light," *Phys. Rev. B* **60**, 9061 (1999).
7. J. R. Krenn et al., "Non-diffraction-limited light transport by gold nanowires," *Europhys. Lett.* **60**, 663–669 (2002).
8. S. A. Maier et al., "Observation of near-field coupling in metal nanoparticle chains using far-field polarization spectroscopy," *Phys. Rev. B* **65**, 193408 (2002).
9. S. A. Maier et al., "Local detection of electromagnetic energy transport below the diffraction limit in metal nanoparticle plasmon waveguides," *Nat. Mater.* **2**, 229–232 (2003).
10. R. Zia et al., "Geometries and materials for subwavelength surface plasmon modes," *J. Opt. Soc. Am. A* **21**, 2242–2246 (2004).
11. J. A. Dionne, L. A. Sweatlock, and H. A. Atwater, "Plasmon slot waveguides: towards chip-scale propagation with subwavelength-scale localization," *Phys. Rev. B* **73**, 035407 (2006).
12. M. L. Brongersma and P. G. Kik, *Surface Plasmon Nanophotonics*, Springer, Dordrecht, The Netherlands (2007).
13. E. N. Economou, "Surface plasmons in thin films," *Phys. Rev.* **182**, 539–554 (1969).
14. G. Veronis et al., "Metal-dielectric-metal plasmonic waveguide devices for manipulating light at the nanoscale," *Chin. Opt. Lett.* **7**, 302–308 (2009).
15. D. F. P. Pile et al., "Theoretical and experimental investigation of strongly localized plasmons on triangular metal wedges for subwavelength waveguiding," *Appl. Phys. Lett.* **87**, 061106 (2005).
16. B. Steinberger et al., "Dielectric stripes on gold as surface plasmon waveguides," *Appl. Phys. Lett.* **88**, 094104 (2006).
17. S. I. Bozhevolnyi et al., "Channel plasmon subwavelength waveguide components including interferometers and ring resonator," *Nature* **440**, 508–511 (2006).
18. M. Z. Alam, J. S. Aitchison, and M. Mojahedi, "A marriage of convenience: hybridization of surface plasmon and dielectric waveguide modes," *Laser Photon. Rev.* **8**, 394–408 (2014).
19. C. V. Naik, V. M. Shalaev, and A. Boltasseva, "Alternative plasmonic materials: beyond gold and silver," *Adv. Mater.* **25**, 3264–3294 (2013).
20. C. Kittel, *Introduction to Solid State Physics*, John Wiley & Sons, New York, NY (1989).
21. S. A. Maier, *Plasmonics: Fundamentals and Applications*, Springer, New York, NY (2007).
22. L. Kazmerski and D. M. Racine, "Growth, environmental, and electrical properties of ultrathin metal films," *J. Appl. Phys.* **46**, 791–795 (1975).
23. P. Clegg, "The optical constants of thin metallic films deposition by evaporation," *Proc. Phys. Soc., London, B* **65**, 774 (1952).
24. G. H. Chan et al., "Plasmonic properties of copper nanoparticles fabricated by nanosphere lithography," *Nano Lett.* **7**, 1947–1952 (2007).
25. H. Bennett et al., "Formation and growth of tarnish on evaporated silver films," *J. Appl. Phys.* **40**, 3351–3360 (1969).

26. A. J. Hoffman et al., "Negative refraction in semiconductor metamaterials," *Nat. Mater.* **6**, 946 (2007).
27. J. Cleary et al., "IR permittivities for silicides and doped silicon," *J. Opt. Soc. Am. B* **27**, 730 (2010).
28. R. E. Peale et al., "Infrared surface plasmon resonance biosensor," presented at *OSA Biomedical*, Miami, Florida (April 2010).
29. R. Soref, J. Hendrickson, and J. W. Cleary, "Mid-to long-wavelength infrared plasmonic-photonics using heavily doped n-Ge/Ge and n-GeSn/GeSn heterostructures," *Opt. Express* **20**, 3814–3824 (2012).
30. D. Adams et al., "Funneling light through a subwavelength aperture with epsilon-near-zero materials," *Phys. Rev. Lett.* **107**, 133901 (2011).
31. M. G. Blaber, M. D. Arnold, and M. J. Ford, "A review of the optical properties of alloys and intermetallics for plasmonics," *J. Phys.: Condens. Matter* **22**, 143201 (2010).
32. G. V. Naik, J. Kim, and A. Boltasseva, "Oxides and nitrides as alternative plasmonic materials in the optical range," *Opt. Mater. Express* **1**, 1090 (2011).
33. J. Cleary et al., "Silicides for infrared surface plasmon resonance biosensors," 2008, http://www.physics.ucf.edu/~rep/conf_pubs/ConfPubs2008/MRSFall2008biosensor.pdf (19 December 2014).
34. M. Wittmer, "Properties and miroelectronic applications of thin films of refractory metal intrides," *J. Vac. Sci. Technol. A* **3**, 1797 (1985).
35. D. Steinmüller-Nethl et al., "Excitation of surface plasmons on titanium nitride films: determination of the dielectric function," *Thin Solid Films* **237**, 277–281 (1994).
36. P. F. Robusto and R. Braunstein, "Optical measurements of the surface plasmon of indium-tin oxide," *Phys. Status Solidi* **119**, 115–168 (1990).
37. C. Rhodes et al., "Surface plasmon resonance in conducting metal oxides," *J. Appl. Phys.* **100**, 054905 (2006).
38. F. Michelotti et al., "Thickness dependence of surface plasmon polariton dispersion in transparent conducting oxide films at 1.55 μm," *Opt. Lett.* **34**, 839–841 (2009).
39. M. A. Noginov et al., "Transparent conductive oxides: plamsonic materials for telecom wavelengths," *Appl. Phys. Lett.* **99**, 021101 (2011).
40. P. R. West et al., "Searching for better plasmonic materials," *Laser Photon. Rev.* **4**, 795–808 (2010).
41. I. Hamberg and C. G. Granqvist, "Evaporated Sn-doped In_2O_3 films: basic optical properties and applications to energy-efficient windows," *J. Appl. Phys.* **60**, R123–R159 (1986).
42. R. G. Gordon, "Criteria for choosing transparent conductors," *MRS Bull.* **25**, 52–57 (2000).
43. T. J. Coutts, D. L. Young, and X. Li, "Characterization of transparent conducting oxides," *MRS Bull.* **25**, 58–65 (2000).
44. J. Hotovy et al., "Sputtered ITO for application in thin-film silicon solar cells: relationship between structural and electric properties," *Appl. Surf. Sci.* **269**, 81–87 (2013).
45. H. Cao et al., "Second harmonic generation in laser ablated zinc oxide thin film," *Appl. Phys. Lett.* **73**, 572 (1998).
46. A. N. Grigorenko, M. Polini, and K. S. Novoselov, "Graphene plasmonics," *Nat. Photonics* **6**, 749–758 (2012).
47. A. Vakil and N. Engheta, "Transformation optics using graphene," *Science* **332**, 1291–1294 (2011).
48. K. Novoselov et al., "A roadmap for graphene," *Nature* **490**, 192–200 (2012).
49. H. Yan et al., "Tunable infrared plasmonic devices using graphene/insulator stacks," *Nat. Nanotechnol.* **7**, 330–334 (2012).
50. Z. Fei et al., "Gate-tuning of graphene plasmons revealed by infrared nano-imaging," *Nature* **487**, 82–85 (2012).
51. N. Papasimakis et al., "Graphene in a photonic metamaterial," *Opt. Express* **18**, 8353 (2010).
52. J. Mannhart and D. G. Schlom, "Oxide interfaces—an opportunity for electronics," *Science* **327**, 1607–1611 (2010).
53. B. Radisavljevic et al., "Single-layer MoS_2 transistors," *Nat. Nanotechnol.* **6**, 147–150 (2011).

54. Z. Fang et al., "A graphene-antenna sandwich photodetector," *Nano Lett.* **12**, 3808 (2012).
55. N. Youngblood et al., "Multifunctional graphene optical modulator and photodetector integrated on silicon waveguides," *Nano Lett.* **14**, 2741–2746 (2014).
56. W. Zhao, K. Shi, and Z. Lu, "Greatly enhanced ultrabroadband light absorption by monolayer graphene," *Opt. Lett.* **38**, 4342–4345 (2013).
57. X. Ling et al., "Can graphene be used as a substrate for Raman enhancement," *Nano Lett.* **10**, 553–561 (2010).
58. Y. Liu et al., "Plasmon resonance enhanced multicolour photodetection by graphene," *Nat. Commun.* **2**, 579 (2011).
59. F. H. L. Koppens, D. E. Chang, and F. J. G. de Abajo, "Graphene plasmonics: a platform for strong light-matter interactions," *Nano Lett.* **11**, 3370–3377 (2011).
60. J. T. Kim and S.-Y. Choi, "Graphene-based plasmonic waveguides for photonic integrated circuits," *Opt. Express* **19**, 24557–24562 (2011).
61. K. F. Mak et al., "Atomically thin MoS_2: a new direct-gap semiconductor," *Phys. Rev. Lett.* **105**, 136805 (2010).
62. R. V. Gorbachev et al., "Hunting for monolayer boron nitride: optical and Raman signatures," *Small* **7**, 465–468 (2011).
63. A. Yariv and P. Yeh, *Photonics: Optical Electronics in Modern Communications*, 6th ed., Chapter 9, Oxford UniversityOxford, United Kingdom (2006).
64. E. L. Wooten et al., "A review of lithium niobate modulators for fiber-optic communication systems," *IEEE J. Sel. Topics Quantum Electron.* **6**, 69–82 (2000).
65. A. Liu et al., "A high-speed silicon optical modulator based on a metal-oxide-semiconductor capacitor," *Nature* **427**, 615 (2004).
66. R. S. Jacobsen et al., "Strained silicon as a new electro-optic material," *Nature* **441**, 199–202 (2006).
67. Q. Xu et al., "Micrometre-scale silicon electro-optic modulator," *Nature*, **435**, 325–327 (2005).
68. T. Baba et al., "50-Gb/s ring-resonator-based silicon modulator," *Opt. Express* **21**, 11869–11876 (2013).
69. D. J. Thomson et al., "Self-aligned silicon ring resonator optical modulator with focused ion beam error correction," *J. Opt. Soc. Am. B* **30**, 445–449 (2013).
70. A. Melikyan et al., "High-speed plasmonic phase modulators," *Nat. Photonics* **8**, 229–233 (2014).
71. J. Schildkraut, "Long-range surface plasmon electrooptic modulator," *Appl. Opt.* **27**, 4587–4590 (1988).
72. T. Nikolajsen, K. Leosson, and S. I. Bozhevolnyi, "Surface plasmon polariton based modulators and switches operating at telecom wavelengths," *Appl. Phys. Lett.* **85**, 5833–5835 (2004).
73. W. Cai, J. White, and M. Brongersma, "Compact, high-speed and power-efficient electro-optic plasmonic modulators," *Nano Lett.* **9**, 4403–4411 (2009).
74. J. A. Dionne et al., "PlasMOStor: a metal-oxide-Si field effect plasmonic modulator," *Nano Lett.* **9**, 897–902 (2009).
75. V. J. Sorger et al., "Ultra-compact silicon nanophotonic modulator with broadband response," *Nanophotonics* **1**, 17–22 (2012).
76. S. K. Pickus et al., "Silicon plasmon modulators: breaking photonic limits," December 2013, http://photonicssociety.org/newsletters/dec13/RH_SiliconPlasmon.html (19 December 2014).
77. Z. Lu and W. Zhao, "Nanoscale electro-optic modulators based on graphene-slot waveguides," *J. Opt. Soc. Am. B* **29**, 1490–1496 (2012).
78. E. Feigenbaum, K. Diest, and H. A. Atwater, "Unity-order index change in transparent conducting oxides at visible frequencies," *Nano Lett.* **10**, 2111–2116 (2010).
79. V. E. Babicheva and A. V. Lavrinenko, "Plasmonic modulator optimized by patterning of active layer and tuning permittivity," *Opt. Commun.* **285**, 5500–5507 (2012).
80. A. Melikyan et al., "Surface plasmon polariton absorption modulator," *Opt. Express* **19**, 8855–8869 (2011).

81. Z. Lu, W. Zhao, and K. Shi, "Ultracompact electro-absorption modulators based on tunable epsilon-near-zero-slot waveguides," *IEEE J. Photonics* **4**, 735–740 (2012).
82. R. A. Pala et al., "A nonvolatile plasmonic switch employing photochromic molecules," *Nano Lett.* **8**, 1506–1510 (2008).
83. D. Pacifici, H. J. Lezec, and H. A. Atwater, "All-optical modulation by plasmonic excitation of CdSe quantum dots," *Nat. Photonics* **1**, 402–406 (2007).
84. C. Min and G. Veronis, "Absorption switches in metal-dielectric-metal plasmonic waveguides," *Opt. Express* **17**, 10757–10766 (2009).
85. K. Shi et al., "Tunable plasmonic metamaterial based on transparent conducting oxide," *Proc. SPIE* **8980**, 898012 (2014).
86. C. Lu et al., "Polymer electrolyte-gated carbon nanotube field-effect transistor," *Nano Lett.* **4**, 623–627 (2004).
87. X. Gan et al., "High-contrast electrooptic modulation of a photonic crystal nanocavity by electrical gating of graphene," *Nano Lett.* **13**, 691–696 (2013).
88. P. Yeh, A. Yariv, and C. S. Hong, "Electromagnetic propagation in periodic stratified media. I. General theory," *J. Opt. Soc. Am.* **67**, 423–438 (1977).
89. K. Shi et al., "Broadband electro-optical modulator based on transparent conducting oxide," *Opt. Lett.* **39**, 4978–4981 (2014).
90. G. D. Wilk, R. M. Wallace, and J. M. Anthony, "High-k gate dielectrics: current status and materials properties considerations," *J. Appl. Phys.* **89**, 5243 (2001).
91. K. Shi, W. Zhao, and Z. Lu, "Epsilon-near-zero-slot waveguides and their applications in ultrafast laser beam steering," *Proc. SPIE* **8980**, 89800L (2014).
92. M. Silveirinha and N. Engheta, "Tunneling of electromagnetic energy through subwavelength channels and bends using ϵ-near-zero materials," *Phys. Rev. Lett.* **97**, 157403 (2006).
93. R. Liu et al., "Experimental demonstration of electromagnetic tunneling through an epsilon-near-zero metamaterial at microwave frequencies," *Phys. Rev. Lett.* **100**, 023903 (2008).
94. R. W. Ziolkowski, "Propagation in and scattering from a matched metamaterial having a zero index of refraction," *Phys. Rev. E* **70**, 046608 (2004).
95. M. Silveirinha and N. Engheta, "Design of matched zero-index metamaterials using nonmagnetic inclusions in epsilon-near-zero media," *Phys. Rev. B* **75**, 075119 (2007).
96. A. Alù et al., "Epsilon-near-zero (ENZ) metamaterials and electromagnetic sources: tailoring the radiation phase pattern," *Phys. Rev. B* **75**, 155410 (2007).
97. S. Enoch et al., "A metamaterial for directive emission," *Phys. Rev. Lett.* **89**, 213902 (2002).
98. L. V. Alekseyev et al., "Uniaxial epsilon-near-zero metamaterial for angular filtering and polarization control," *Appl. Phys. Lett.* **97**, 131107 (2010).
99. V. Mocella et al., "An extraordinary directive radiation based on optical antimatter at near infrared," *Opt. Express* **18**, 25068–25074 (2010).
100. A. Ciattoni et al., "ϵ-near-zero materials in the near-infrared," *Appl. Phys. B* **110**, 23–26 (2013).
101. V. R. Almeida et al., "Guiding and confining light in void nanostructure," *Opt. Lett.* **29**, 1209–1211 (2004).
102. Q. Xu, V. R. Almeida, and M. Lipson, "Experimental demonstration of guiding and confining light in nanometer-size low-refractive-index material," *Opt. Lett.* **29**, 1626–1628 (2004).
103. Z. Lu, W. Zhao, and K. Shi, "Nanoscale plasmonic and optical modulators based on transparent conducting oxides," arXiv:1205.0502v1 (2012).
104. H. D. Tholl, "Novel laser beam steering techniques," *Proc. SPIE* **6397**, 639708 (2006).
105. J. Bourderionnet et al., "Continuous laser beam steering with micro-optical arrays—experimental results," *Proc. SPIE* **7113**, 71130Z (2008).
106. J. Kim et al., "Wide-angle, nonmechanical beam steering using thin liquid crystal polarization gratings," *Proc. SPIE* **7093**, 709302 (2008).

Kaifeng Shi obtained his bachelor's degree from Beihang University, Beijing, in 2010 and his master's degree in electrical engineering from the University of South Carolina in 2012. He then joined Dr. Zhaolin Lu's group in Microsystems Engineering at RIT. He is now a third-year PhD student and mainly working on graphene absorption and novel electro-optical modulators.

Zhaolin Lu is an associate professor of microsystems engineering PhD program and Department of Electrical and Microelectronic Engineering at RIT. He obtained his PhD degree in electrical engineering from the University of Delaware and joined RIT in 2007, where he established the Novel Material Photonics Laboratory. Activities within the laboratory are directed toward the exploration of novel materials and nanostructures for applications in the fields of nanophotonics, optical communications, super-resolution imaging, renewable energy, etc.